Reprinted from

EARTH AND PLANETARY SCIENCE LETTERS

Earth and Planetary Science Letters 171 (1999) 647–660

Erosional history of the Himalayan and Burman ranges during the last two glacial–interglacial cycles

C. Colin [a,*], L. Turpin [b], J. Bertaux [c], A. Desprairies [a], C. Kissel [b]

[a] *Laboratoire de Géochimie des Roches Sédimentaires, Université Paris-Sud, 91405 Orsay Cedex, France*
[b] *Laboratoire des Sciences du Climat et de l'Environnement, Laboratoire mixte CNRS–CEA, Avenue de la Terrasse, 91198 Gif-sur-Yvette Cedex, France*
[c] *Centre ORSTOM, 72 route d'Aulnay, 93143 Bondy Cedex, France*

Received 14 July 1998; accepted 13 July 1999

ELSEVIER

Earth and Planetary Science Letters 171 (1999) 647–660

EPSL

www.elsevier.com/locate/epsl

Erosional history of the Himalayan and Burman ranges during the last two glacial–interglacial cycles

C. Colin [a,*], L. Turpin [b], J. Bertaux [c], A. Desprairies [a], C. Kissel [b]

[a] *Laboratoire de Géochimie des Roches Sédimentaires, Université Paris-Sud, 91405 Orsay Cedex, France*
[b] *Laboratoire des Sciences du Climat et de l'Environnement, Laboratoire mixte CNRS–CEA, Avenue de la Terrasse, 91198 Gif-sur-Yvette Cedex, France*
[c] *Centre ORSTOM, 72 route d'Aulnay, 93143 Bondy Cedex, France*

Received 14 July 1998; accepted 13 July 1999

Abstract

The results of a clay mineralogy study combined with major element geochemistry, strontium, neodymium and oxygen isotopes, and ^{14}C AMS stratigraphy are reported for deep-sea gravity cores located in the Bay of Bengal (MD77-180) and the Andaman Sea (MD77-169). $\varepsilon_{Nd}(0)$ and $^{87}Sr/^{86}Sr$ from Holocene and last glacial maximum (LGM) sediments of fifteen other cores have also been investigated to identify sediment sources and to estimate oceanic sedimentary transport. The data show the contribution of three sources: (1) Ganges/Brahmaputra rivèrs; (2) Irrawaddy River; and (3) sediment derived from the western part of the Indo–Burman ranges. The dispersion of the detrital material issuing from these sources has been constrained by the geographic distribution of Nd and Sr isotopic ratios. The LGM sediments are characterized by a significant increase of $^{87}Sr/^{86}Sr$, small changes in $\varepsilon_{Nd}(0)$, and a general decrease of smectite/(illite + chlorite), which together imply a decrease in weathering intensity. The increased $^{87}Sr/^{86}Sr$ are attributed to a decrease in chemical weathering, which should release preferentially ^{87}Sr during weathering processes. In the Andaman Sea sediments, smectite/(illite + chlorite) and kaolinite/quartz ratios combined with a chemical index of alteration (CIA*) indicate that the weathering intensity of the Irrawaddy River basin is mainly controlled by the summer monsoon rainfall intensity. The wet summer monsoons increase vegetation cover in the plains and favor soil development by the production of pedogenic clays (smectite and kaolinite).

Keywords: monsoons; deep-sea sedimentation; erosion; Burman ranges; Himalayas

1. Introduction

The Himalaya has one of the world's highest physical and chemical erosion rates [1,2] and thus constitute an interesting region to establish a relationship between erosion and climate. Over geological time scales, changes in the strength of the summer monsoon rainfall represent an important factor driving weathering and erosion of the Himalaya. Sediments of the Bay of Bengal and Andaman Sea, which are fed by the Ganges/Brahmaputra and Irrawaddy rivers, thus provide an exceptional record of the variability of the intensity of erosion in the Himalayan and Burman ranges. This in turn is related to paleoclimatic and paleoenvironmental changes affecting SW Asia.

Previous studies, based on cores retrieved from

* Corresponding author. Tel.: +33 1 6915 6745; Fax: +33 1 6915 4882; E-mail: colin@geol.u-psud.fr

0012-821X/99/$ – see front matter
PII: S0012-821X(99)00184-3

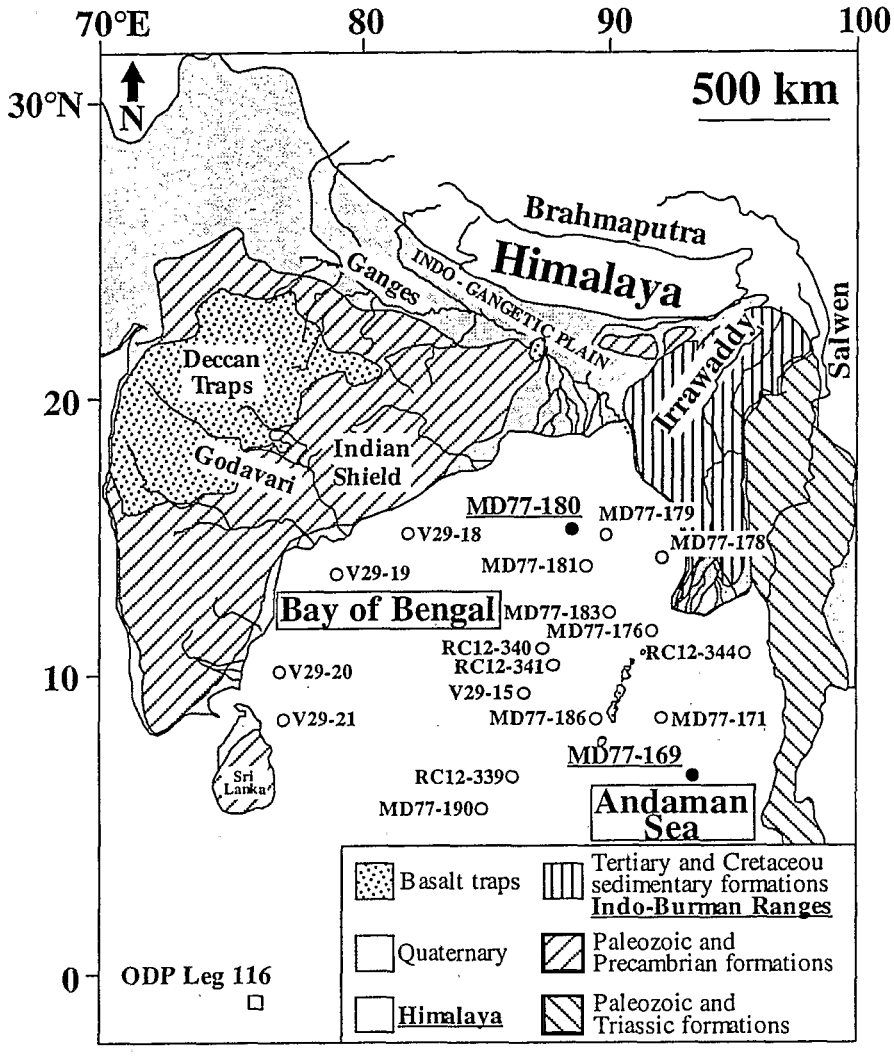

Fig. 1. Schematic geological map of the Indian subcontinent and location of the studied cores. The two cores investigated in detail in this study are underlined. The seventeen other cores are geographically distributed to ensure a good coverage of the Bay of Bengal and the Andaman Sea.

the distal portion of the Bengal Fan (ODP Leg 116, Fig. 1), allowed the reconstruction of the erosional history of the Himalayan–Tibetan complex since the Early Miocene (last 20 Ma) [3–10]. Variations in the erosion rate of the Himalaya–Tibet complex over such time scales have been shown to depend on several factors, including paleoclimatic/paleoenvironmental changes and tectonic activity.

This paper reports on a high-resolution study of clay mineralogy and major element geochemistry of two deep-sea gravity cores from the Bay of Bengal (MD77-180) and Andaman Sea (MD77-169). These were analyzed to reconstruct the erosional history of the Himalayan and Burman ranges over the last two climatic cycles (last 280 kyr). This shorter time scale is independent of major tectonic activity and permits us to establish a relationship between past changes in the intensity of the Indian monsoon rainfall [11–14] and the intensity of chemical and physical weathering in the Himalayan and Burman ranges. However, past changes in the Indian summer monsoon intensity have also impacted the sea surface circulation in the Bay of Bengal and the Andaman Sea [11,12]. This may affect oceanic sedimentary transport and thus modify the source, grain size, and composition of sediment at a given site.

To determine the sediment sources and assess the effects of oceanic transport in the sedimentary record, we have also investigated Nd and Sr isotopes

in several Holocene and LGM sediments distributed throughout the Bay of Bengal and Andaman Sea. Clay mineralogy, major element compositions and spectral analysis of the two deep-sea cores recovered from the Bay of Bengal and Andaman Sea permit us to establish the impact of climatic and sea level changes on the weathering and erosion of the Himalayan and Burman ranges.

2. Materials and methods

2.1. Cores location and sampling

The deep-sea gravity cores investigated here are plotted in Fig. 1, and their characteristics are given in Table 1. Two cores from the MD77 cruise were studied in detail: MD77-169 and MD77-180. Core MD77-169 was taken on the Sewell Seamount, central Andaman Sea, in order to avoid slope deposits such as turbidites or slumping. The lithology is homogeneous, dominated by terrigenous muddy clay and nannofossil carbonate ooze. Core MD77-180 was taken near the continental slope (about 100 miles off the coast) (Fig. 1) and is characterized by intercalated clay and silty clay layers. These two cores were sampled at 10- to 20-cm intervals for the mineralogical and geochemical investigations. Fifteen other cores, selected to cover the Bay of Bengal and Andaman Sea (Fig. 1 and Table 1), were sampled only at the top and the Last Glacial Maximum (LGM) in order to establish the spatial distribution of Sr and Nd isotopes during these two periods.

2.2. Methods

Sr and Nd isotopic measurements were performed on the carbonate free fraction. Samples were decarbonated by leaching with 20% acetic acid in an ultrasonic bath, then rinsed 5 times and centrifuged to eliminate traces of the carbonate solution. Samples were dissolved in HF–$HClO_4$ and HNO_3–HCl mixtures. A first chemical separation used Biorad columns packed with AG50WX-8, 200–400 mesh cationic exchange resin. Sr and Rb were eluted with 2 N HCl and the light rare earth elements with 2.5 N HNO_3. The Sr fraction was purified on a 20-μl SrSpec® column consisting of a polyethylene syringe with a 4 mm Ø millex® filter. Nd was isolated by reverse-phase chromatography on HDEHP-coated Teflon powder. Isotopic measurements were performed using static multicollection on a Finnigan MAT-262. Repeated analysis of NIST SRM987 during the study gave a mean $^{87}Sr/^{86}Sr$ of 0.710237 ± 0.000007 (2 σ). The mean $^{143}Nd/^{144}Nd$ for a Johnson Matthey internal lab standard from A. Michard was 0.511093 ± 0.000005, which corresponds to a value of 0.511845 for La Jolla.

Clay mineralogy determinations were made by standard X-ray diffraction [15] on the carbonate-free, <2 μm size fraction. Samples were split in deionized water and decarbonated in 0.2 N HCl. The integrity of the clay fraction after acid leaching was controlled by observations on a transmission electron microscopy and X-ray diffraction patterns of bulk samples. The <2 μm clay fraction was isolated by gravity settling [15]. X-ray diffractograms were made on a INEL CPS 120 X-ray diffractometer from 2.49° to 32.5° using a cobalt $K\alpha_1$ radiation. Three tests were performed on the oriented mounts: (1) untreated; (2) glycolated (12 h in ethylene–gycol); and (3) heated at 540° for 2 h. X-ray diffraction identified: illite, chlorite, kaolinite, smectite and complex mixed-layers. These mixed-layer clays were mainly assigned to randomly mixed illite–smectite species with predominantly smectite layers. These will be referred to as 'smectites' in the text. The semiquantitative composition of the clay fraction was obtained either by measuring the height of basal reflections on XRD diagrams or by measurement of peak areas. The basal reflection heights were weighted by empirically estimated factors [15]: the smectite 17 Å peak height is multiplied by 1.5, the kaolinite 3.6 Å peak by 0.7 and both the illite 10 Å peak and chlorite 3.55 Å peak by 1.

Kaolinite, quartz, and carbonate content of the bulk fraction were determined by Fourier Transform Infra-Red (FTIR) spectroscopy [16]. The samples were ground under acetone to a particle size of less than 2 μm with small agate balls in an agate vial, and kept at 4°C to prevent heating and structural changes. The powder was mixed with KBr in an agate mortar with a dilution factor of 0.25%. A 300 mg pellet, 13 mm in diameter, was pressed into a vacuum die with up to 8 ton/cm^2 of compression. 50 scans of IR spectra per sample cumulated in the 4000–250

Table 1
Core locations, sample depths and Sr and Nd isotope data

Core number	Lat.	Long.	Water depth (m)	Depth (cm)	Isotopic stages	Sr (ppm)	$^{87}Sr/^{86}Sr$	Nd (ppm)	$^{143}Nd/^{144}Nd$	$\varepsilon_{Nd}(0)$
Irrawaddy sediment						188.0	0.71333	30.5	0.512091	−10.7
MD77-169	10°12′5 N	95°03′0 E	2360	24	Holocene	129.7	0.71434	24.0	0.512125	−10.0
MD77-169				158	LGM	110.4	0.71669	23.5	0.512095	−10.6
MD77-171	11°45′6 N	94°09′0 E	1760	47	Holocene	162.8	0.71233	21.5	0.512164	−9.2
MD77-171				265	LGM	98.1	0.71332	17.0	0.512187	−8.8
MD77-176	14°30′5 N	93°07′6 E	1375	17	Holocene	113.0	0.71534	24.2	0.512162	−9.3
MD77-176				590	LGM	90.9	0.71777	22.7	0.512209	−8.4
MD77-178	17°11′7 N	93°05′0 E	2459	60	Holocene	98.9	0.71453	16.8	0.512199	−8.6
MD77-178				240	LGM	94.2	0.71613	20.2	0.512277	−7.0
MD77-179	18°21′6 N	91°01′3 E	1986	3	Holocene	127.5	0.71998	24.3	0.511981	−12.8
MD77-179				41	LGM	106.3	0.72101	32.0	0.512088	−10.7
MD77-180	18°28′3 N	89°51′4 E	1986	84	Holocene	100.5	0.72587	30.3	0.511993	−12.6
MD77-180				200	LGM	91.5	0.72315	34.0	0.512074	−11.0
MD77-181	17°23′7 N	90°29′1 E	2271	13	Holocene	127.6	0.71990	26.5	0.511998	−12.5
MD77-181				165	LGM	94.5	0.72135	30.2	0.512115	−10.2
MD77-183	15°09′0 N	91°43′0 E	2632	27	Holocene	126.7	0.71467	26.3	0.512175	−9.0
MD77-183				175	LGM	88.7	0.71914	28.1	0.512200	−8.6
MD77-186	11°27′5 N	92°00′0 E	890	90	Holocene	142.1	0.71498	23.6	0.512081	−10.9
MD77-186				240	LGM	116.4	0.71683	26.5	0.512114	−10.2
MD77-190	07°41′0 N	87°49′6 E	3742	11	Holocene	174.5	0.71380	24.1	0.512088	−10.7
RC12-339	09°08′ N	90°02′ E	3010	4	Holocene	194.2	0.71433	23.6	0.512048	−11.5
RC12-339				101	LGM	142.6	0.71574	24.2	0.512118	−10.1
RC12-340	12°42′ N	90°01′ E	3012	8	Holocene	149.2	0.71571	25.2	0.512105	−10.4
RC12-340				70	LGM	112.5	0.71789	29.3	0.512152	−9.5
RC12-341	13°03′ N	89°35′ E	2988	12	Holocene	162.7	0.71379	21.4	0.512111	−10.3
RC12-341				60	LGM	96.7	0.71799	27.8	0.512195	−8.6
RC12-344	12°46′ N	96°04′ E	2140	25	Holocene	106.3	0.71719	29.1	0.512059	−11.3
RC12-344				320	LGM	84.6	0.72230	28.5	0.512048	−11.5
VM29-15	11°57′ N	88°44′ E	3173	5	Holocene	228.4	0.71232	19.9	0.512085	−10.8
VM29-15				72	LGM	152.8	0.71634	23.2	0.512129	−9.9
VM29-18	16°38′ N	85°24′ E	2816	3	Holocene	106.4	0.72411	27.5	0.511866	−15.1
VM29-19	14°42′ N	83°35′ E	3182	8	Holocene	76.8	0.72305	21.0	0.511924	−13.9
VM29-20	11°32′ N	81°42′ E	3557	10	Holocene	82.0	0.72576	25.6	0.511811	−16.1
VM29-21	09°39′ N	81°45′ E	3724	2	Holocene	71.1	0.73156	25.1	0.511809	−16.2

The deep sea gravity cores were collected in the Andaman Sea and the Bay of Bengal during the OSIRIS III expedition of the French R/V *Marion Dufresne* in 1977 (MD77 cores), or were obtained from Lamont Doherty Geological Observatory collections (V29 and RC12 cores).
$\varepsilon_{Nd}(0) = [^{143}Nd/^{144}Nd_{meas}/0.512638 - 1] \times 1000$ using the present CHUR value of Jacobsen and Wasserburg [35].

cm^{-1} energy range with a 2 cm^{-1} resolution, using a Perkin-Elmer FT 16 PC spectrometer. Kaolinite and quartz proportions have been corrected for carbonate dilution.

The major element determinations were performed on a microprobe JEOL JS-840 coupled with a EDXA-LinK KZ-5 after fusion of the carbonate free-fraction following the procedure described by Colin et al. [17].

3. Chronological framework

The stratigraphy of core MD77-169 has been established using thirteen Accelerator Mass Spectrometry (AMS) ^{14}C dates (based on monospecific samples of planktonic *G. ruber*) and the $\delta^{18}O$ from planktonic foraminifera *G. ruber*, using the SPECMAP reference time scale [11,17] (Fig. 2). This core provides a continuous sedimentary record extending

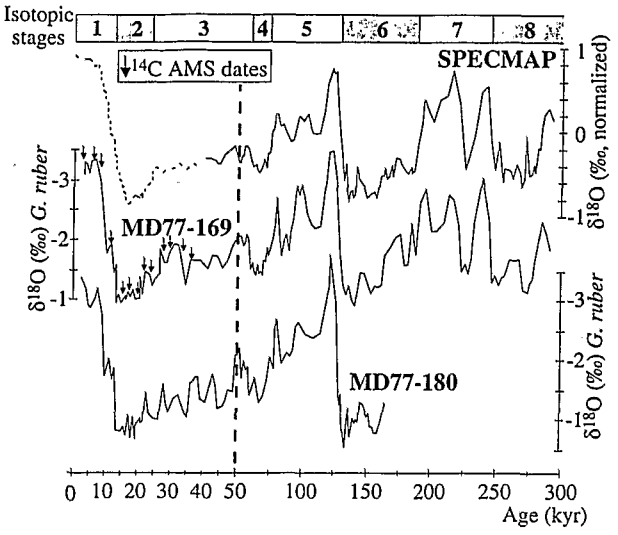

Fig. 2. Planktonic foraminifera *G. ruber* $\delta^{18}O$ record of cores MD77-169 and MD77-180. The time scale of core MD77-169 has been obtained combining ^{14}C AMS ages and correlation with the SPECMAP isotopic record of Martinson et al. [34]. The time scale of core MD77-180 has been obtained using the planktonic foraminifera $\delta^{18}O$ record of core MD77-169 as reference. Isotopic stages 7, 5 and 1 are considered as interglacial periods and isotopic stages 8, 6, 4, 3 and 2 as glacial periods. Note change in scale after 50 kyr.

down to climate stage 8 with an average sedimentation rate around 10.9 cm/kyr for the last 74 kyr and 3.9 cm/kyr for the bottom (Fig. 3).

Time scales of all the other cores were established using $\sigma^{18}O$ of *G. ruber* using MD77-169 as reference and the Toba ash layer dated at 74 ± 2 kyr [18,19] as a tie-point. In core MD77-180, the sedimentary sequences represent the last climatic stage (about 160 kyr) (Fig. 2). This core is characterized by higher accumulation rates during glacial stages 2, 3, 4 and 6 (around 7.7 and 11.7 cm/kyr) than during interglacial stage 5 (around 4 cm/kyr) (Fig. 3). The oxygen isotope stratigraphy established for the fifteen other cores permits to unambiguously recognize the Holocene and the LGM levels [11].

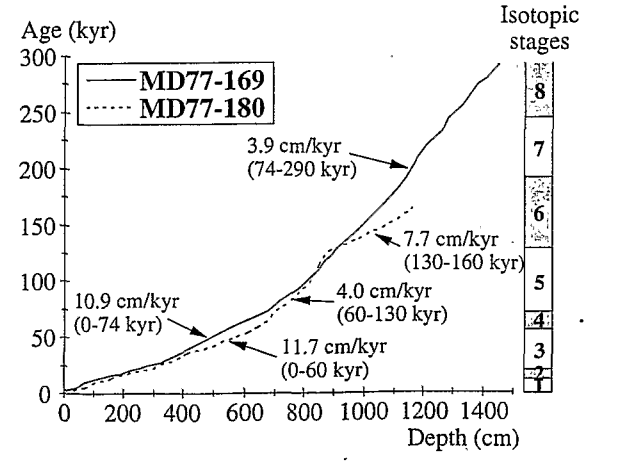

Fig. 3. Depth (cm) versus age (kyr) diagram showing variations of the sedimentation rate for the two cores. Average sedimentation rates of different parts of these two cores are also given.

4. Results

4.1. Isotopic results

Nd and Sr concentrations and isotopic ratios are listed in Table 1. The ranges of Nd and Sr concentrations, 17–34 ppm Nd and 71–228 ppm Sr, are normal relative to the previously published Ganges–Brahmaputra and Bay of Bengal data [3,6,20].

For the Holocene sediments (Fig. 4a), $\varepsilon_{Nd}(0)$ values range from −8.6 to −16.2 and $^{87}Sr/^{86}Sr$ ranges from 0.712 to 0.732. The data allow the sediments located in the western Bay of Bengal to be clearly distinguished from those from the eastern Bay of Bengal and Andaman Sea. Western Bay of Bengal samples show $\varepsilon_{Nd}(0)$ ranging between −13.9 and −16.2 and $^{87}Sr/^{86}Sr$ between 0.723 and 0.732 (Fig. 4a). Holocene sediments sampled near the Ganges–Brahmaputra mouth (northern Bay of Bengal) have $\varepsilon_{Nd}(0)$ between −12.5 and −12.8 and $^{87}Sr/^{86}Sr$ between 0.720 and 0.726. Such values are different from those given by the Ganges River sediments [3,6,10], suggesting the involvement of an additional detrital source. With the exception of core MD77-171, the Holocene sediments of the Andaman Sea give $\varepsilon_{Nd}(0)$ values between −10 and −11.3 and $^{87}Sr/^{86}Sr$ ratios between 0.714 and 0.717; these values are similar to an Irrawaddy River sample ($\varepsilon_{Nd}(0) = -10.7$; $^{87}Sr/^{86}Sr = 0.713$). Sediments off the Arakan coast (Fig. 4a) and between the Andaman Sea and the Bay of Bengal are characterized by higher $\varepsilon_{Nd}(0)$ values close to −8.6, with a geographical distribution showing a tongue-shaped pattern following a NE–SW axis; such a pattern is not observed with $^{87}Sr/^{86}Sr$.

The Andaman Sea sediments present a similar isotopic distribution during LGM and Holocene although the $^{87}Sr/^{86}Sr$ ratios are slightly higher

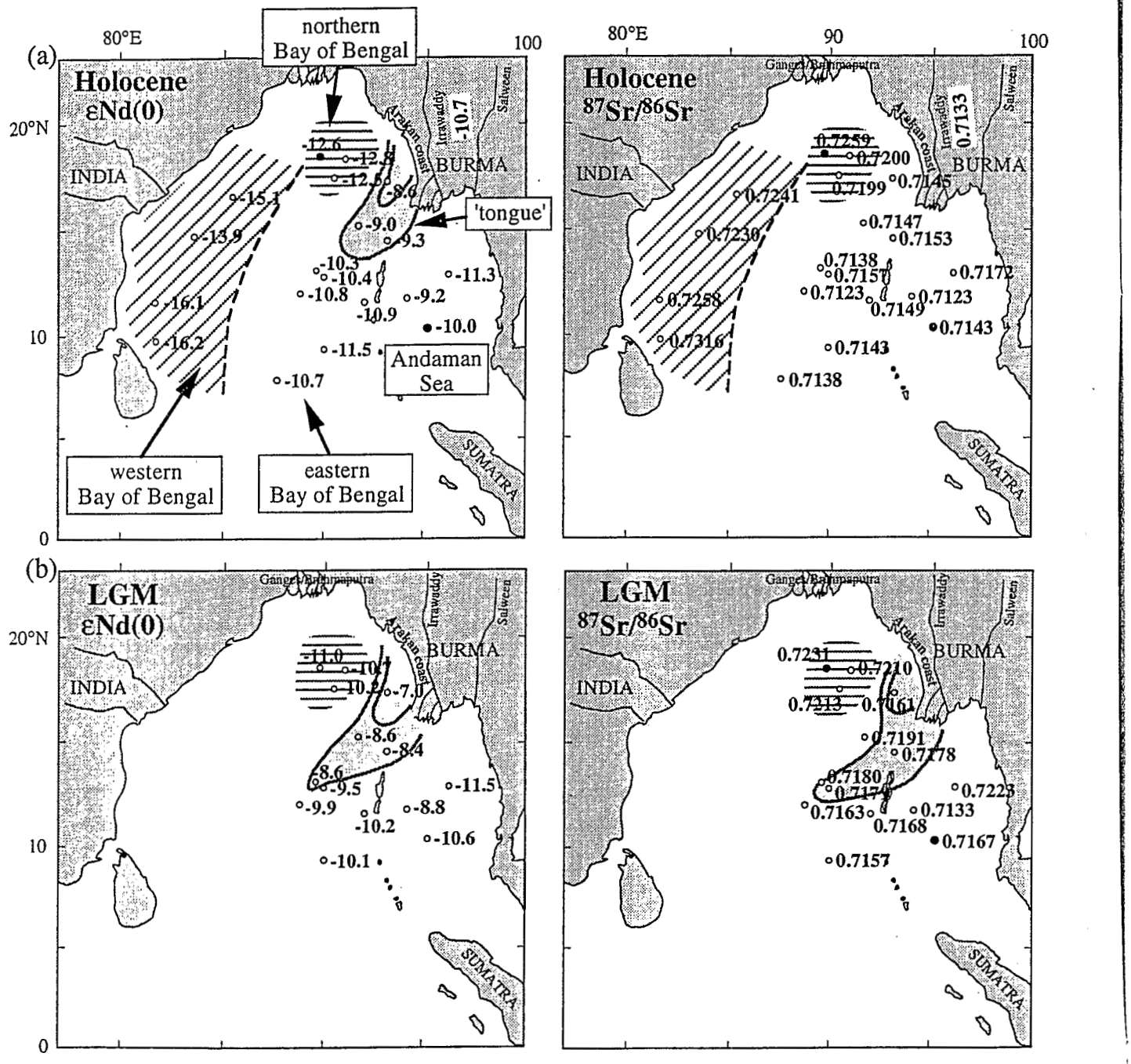

Fig. 4. Spatial distribution of $\varepsilon_{Nd}(0)$ values and $^{87}Sr/^{86}Sr$ isotopic ratios for the Holocene (a) and LGM (b) sediments. Filled in symbols are two cores analysed in detail.

(Fig. 4b). On the contrary, the isotopic ratios of sediments located between the Andaman Sea and the Bay of Bengal are different in the LGM and at the Holocene. The geographical distribution of the $\varepsilon_{Nd}(0)$ values and $^{87}Sr/^{86}Sr$ ratios present the same 'tongue'. The LGM is characterized by little change in $\varepsilon_{Nd}(0)$ but a significant increase in $^{87}Sr/^{86}Sr$.

4.2. Mineralogy results

In core **MD77-169**, the illite and chlorite distributions are similar and inversely correlated to the smectite distribution (Fig. 5b). The smectite content ranges between 20 and 60% with higher values during the last 60 kyr. Prior to 60 kyr, the

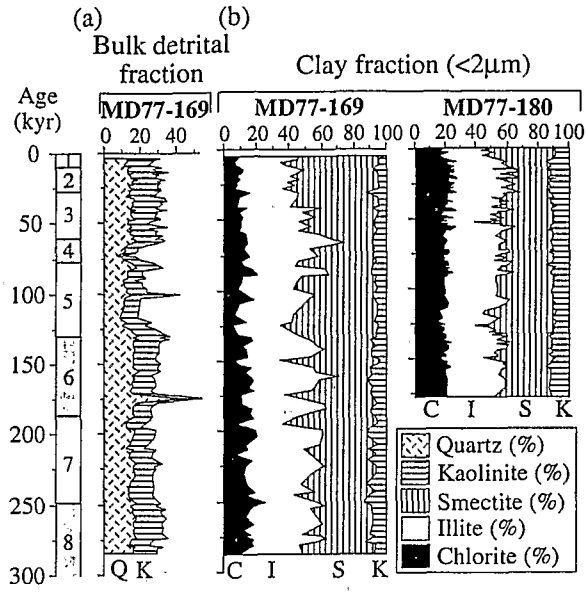

Fig. 5. (a) Quartz and kaolinite proportions (%) on the bulk detrital fraction versus age (kyr) for core MD77-169. (b) Clay minerals proportion (%) on the <2 μm size fraction versus age (kyr) for cores MD77-169 and MD77-180. Isotopic stages are also reported.

smectite distribution shows several peaks (Fig. 5b) also observed in the (smectite)/(illite + chlorite) ratio (Fig. 6b). The kaolinite content of the <2 μm size fraction, as determined by X-ray diffraction, does not vary significantly along the core. Long-term fluctuations of quartz and kaolinite of the bulk detrital fraction, performed by FTIR analyses, are similar and show lower values during interglacial stage 5 (Fig. 5a). Downcore variations of the kaolinite/quartz ratio show a distribution pattern similar to the smectite/(illite + chlorite) ratio (Fig. 6b) with higher values in the upper part of the core and the same peaks during time interval 60–260 kyr.

A spectral analysis has been performed using the Analyserie software [21] on the smectite/(illite + chlorite) and kaolinite/quartz ratio records for this core which present the longest time record. The power density spectrum reported in Fig. 7 shows significant periodicities at 23 and 100 kyr for the smectite/(illite + chlorite) ratio and at 23 and 142 kyr for the kaolinite/quartz ratio. Periodicity at 23 kyr is attributed to the precessional changes of the earth's orbit, and periodicities close to 100 kyr are related to long-term changes of the ice-volume. The periodicity of ca. 40 kyr of the obliquity change is not observed in this core. Changes in these two ratios show congruent precession-related (23 kyr) oscillations correlating the mineralogical characteristics with the solar radiation calculated at 10°N for September (the month which is in phase with clay mineralogy variations) (Fig. 6a,b). This feature is particularly well marked during the time interval 60–240 kyr. This suggests that smectite/(illite + chlorite) and kaolinite/quartz ratio variations are strongly related to the changes of the SW monsoon.

Although core **MD77-180** is fed by a different river system than core MD77-169, the clay assemblage of this core is also characterized by an opposite behavior of smectite and illite–chlorite (Fig. 5b). The smectite/(illite + chlorite) ratio is higher during isotopic stages 1 and 5e, as well as around 55 and 145 kyr during glacial periods (Fig. 6c).

4.3. Major element results

Major element determination was performed only in core MD77-169. A modified chemical index of alteration has been calculated from the major element results using: $CIA^* = [Al_2O_3/(Al_2O_3 + Na_2O + K_2O] \times 100$. This parameter, introduced by Nesbitt and Young [22], quantifies the intensity of cation loss during weathering, and reflects the proportions of primary and secondary minerals in bulk samples. However, we have not used the Ca element for CIA calculation because this element does not present any significant variations.

CIA^* values obtained from core MD77-169 range between 81% and 85%, suggesting very limited changes in the chemical weathering of the detrital material (Fig. 6b). However, a detailed examination of this curve shows a good correlation of the CIA^* with the kaolinite/quartz ratio and to a lesser extent with the smectite/(illite + chlorite) ratio.

5. Discussion

5.1. Holocene sediment sources

The $^{87}Sr/^{86}Sr$ ratios versus $\varepsilon_{Nd}(0)$ measured for the Holocene and LGM sediments are presented in Fig. 8, together with data of the ODP Leg 116 sediments [3,6,10] and fields of major Himalayan

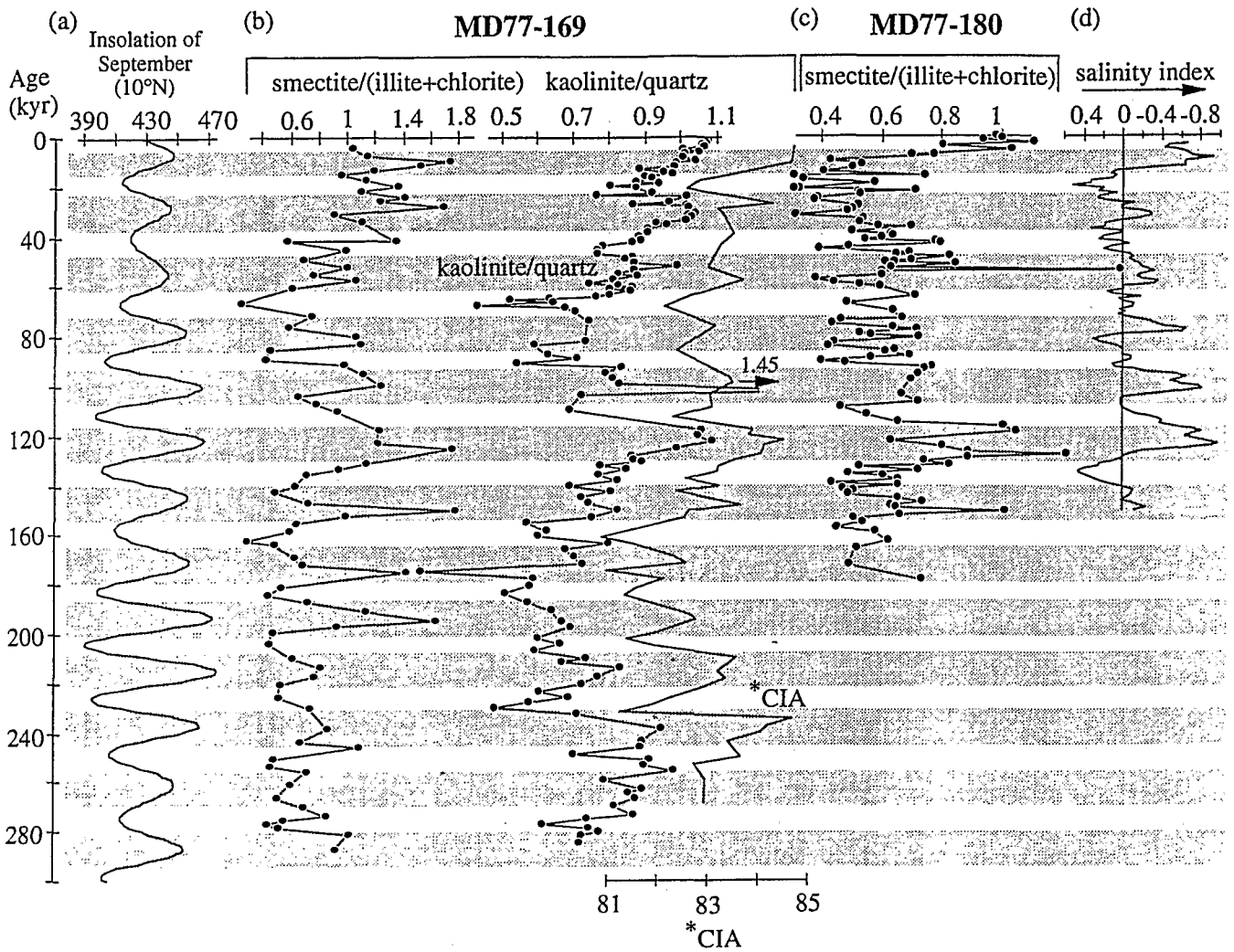

Fig. 6. Insolation curve calculated for the month of September at latitude of 10°N (using Analyserie software [21] (a); smectite/(illite + chlorite) and kaolinite/quartz ratios and the chemical index alteration (CIA* = molar ratio of $[Al_2O_3/(Al_2O_3 + Na_2O + K_2O] \times 100$) versus age (kyr) for core MD77-169 (b); smectite/(illite + chlorite) ratio versus age (kyr) for core MD77-180 (c); salinity gradient between the Andaman Sea and Banda Sea plotted versus age (kyr) [33] obtained on the $\delta^{18}O$ difference of *G. ruber* between cores MD77-169 and SHI90-14 (Banda Sea, water depth of 3163 m, 5°46′S 126°58′E) (d). Shaded bands denote intervals of maximum insolation.

formations [23]. Data are presented in more detail for the Holocene and LGM sediments in Fig. 9. In such diagrams, mixing of sediments from two different sources generates a hyperbolic trend between end-members, the shape of which depends on end-member Sr/Nd ratios. It is worth noting that as long as source rocks have similar Sr/Nd and the sedimentary products experienced similar weathering histories, their Sr/Nd ratios will be similar and the curvature of their mixing hyperbolae will be low. While the Sr and Nd isotopes data from the ODP Leg 116 samples are in the range defined by the primary rocks from the High Himalaya Crystalline (HHC) [3,6,10], our gravity core sediments fall in the field of the High Himalaya Sedimentary Series (HHSS) (Fig. 8). This implies that sediments deposited on the axis of the Bengal Fan have a different source than those deposited in the Bay of Bengal. In the region studied, several areas can be distinguished: (1) western Bay of Bengal, (2) northern Bay of Bengal; (3) eastern Bay of Bengal/Andaman Sea; and (4) the 'tongue' (Figs. 4 and 9).

Sediments from the western Bay of Bengal have $\varepsilon_{Nd}(0)$ similar to those of ODP Leg 116 [3,6] and of Ganges sediments [20], but with significantly lower $^{87}Sr/^{86}Sr$ ratios (Figs. 8 and 9a). Such features are in-

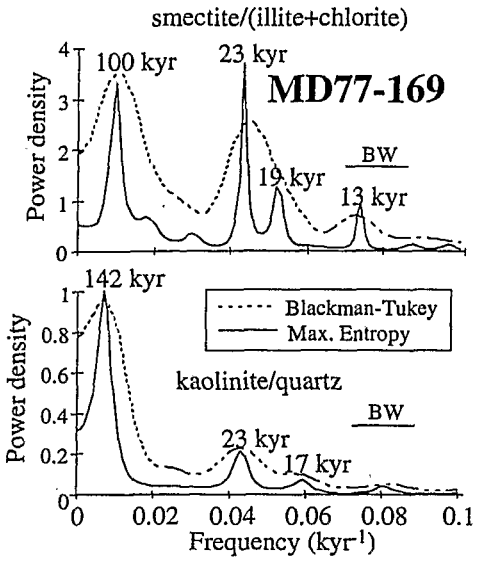

Fig. 7. Periodograms of the smectite/(illite + chlorite) and kaolinite/quartz ratios for core MD77-169. Dashed line=Blackman–Tukey; solid line = maximum entropy; *BW* =is the bandwidth.

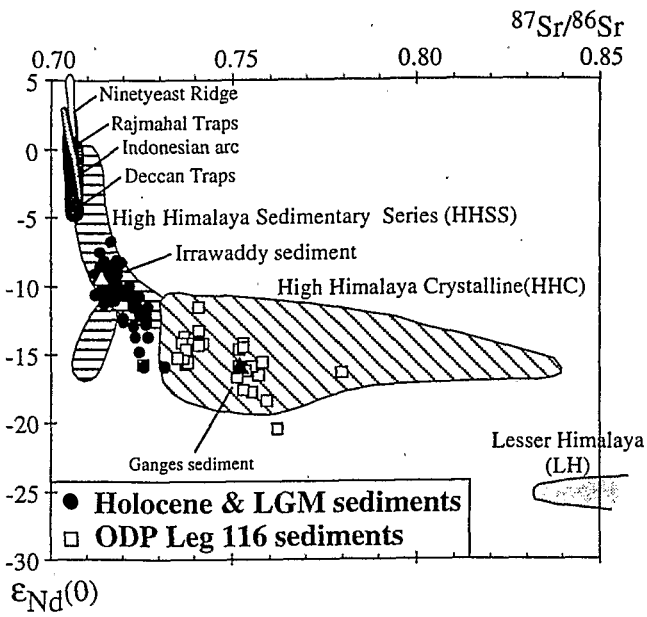

Fig. 8. $^{87}Sr/^{86}Sr$ isotopic ratios versus $\varepsilon_{Nd}(0)$ diagram for the Holocene and LGM sediments. Sr and Nd isotopes compositions of the ODP Leg 116 sediments located in the distal portion of the Bengal Fan and of the major potential Himalayan sources [23] are also reported for comparison.

terpreted as follows. The main sedimentary source is the Ganges–Brahmaputra Rivers mixed with an additional component from younger continental crust, with higher Sr and lower Nd contents. Such a component can be derived from the Deccan Traps. Previous

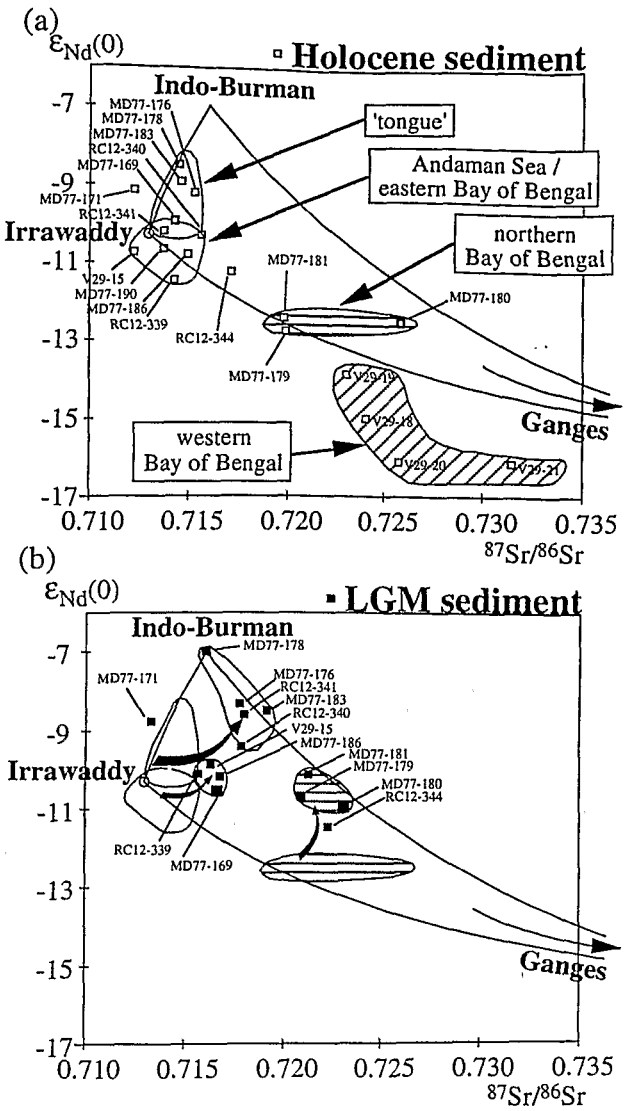

Fig. 9. $^{87}Sr/^{86}Sr$ isotopic ratios versus $\varepsilon_{Nd}(0)$ diagram for the Holocene (a) and LGM (b) sediments. *Irrawaddy* = Irrawaddy River; *Indo–Burman* = western part of the Indo–Burman ranges; *Ganges* = Ganges/Brahmaputra rivers.

investigations have reported that such material could be provided to the ocean by rivers such as the Godavari, which find their sources in the Deccan Traps (Fig. 1) and transport high smectite content deriving from basaltic material weathering [24–26].

From their isotopic characteristics, the Holocene sediments recovered in the rest of the Bay of Bengal and the Andaman Sea are interpreted as derived by mixing from three potential isotopic end-members (Fig. 9a). The two first correspond to the isotopic composition of sediments recovered in the Irrawaddy River ($\varepsilon_{Nd}(0) \approx -11$; $^{87}Sr/^{86}Sr \approx 0.713$)

and the Ganges River with ($\varepsilon_{Nd}(0) < -15$; $^{87}Sr/^{86}Sr > 0.735$). The third end-member defined using core MD77-178 during the LGM ($\varepsilon_{Nd}(0) = -7$; $^{87}Sr/^{86}Sr = 0.716$) is located close to the Arakan coast (Fig. 4). This end-member is interpreted as deriving from detrital material generated by the erosion of the western part of the Indo–Burman ranges, along the Arakan coast (Fig. 1). Unfortunately, no Nd and Sr isotopic compositions are available for either the primary rocks or the sediments from this area. This part of the Indo–Burman ranges consists of Cretaceous and Oligocene sedimentary shales hosting volcanic dykes and ophiolites [27]. In addition, Paleocene to Oligocene formations, deposited before the uplift of the Himalaya, consist mainly of flysch derived from the eroded material of the Inner Volcanic Arc of Burma [27]. Thus, the position of the third end-member in the Fig. 9 is plausible.

Sediments from the Andaman Sea present a more restricted isotopic range close to the isotopic signature of Irrawaddy River sediment. The Irrawaddy River thus appears as the main contributor of detrital material to the Andaman Sea. The contribution of the Andaman Sea volcanoes is negligible, except for core MD77-171, which is situated on the Alcock Seamount close to the Barren volcanoes. During the Holocene, the Nd and Sr data from the NE–SW tongue-shaped area plot between the Irrawaddy and the Indo–Burman end-members.

5.2. LGM situation

During the LGM, $\varepsilon_{Nd}(0)$ stays roughly the same, whereas $^{87}Sr/^{86}Sr$ increases (Figs. 4 and 9b). Such a change may be explained by either (1) a change of sedimentary sources due to changes in oceanic transport, and/or (2) a change of isotopic composition of terrigenous supply from rivers due to either a change in mechanical vs. chemical weathering or a change in erosion due to glacial/interglacial sea level variations.

Conversely, as LGM sediments in the 'tongue' plot on a hyperbola branch which links the Indo–Burman and Ganges end-members (Fig. 9b), the main contributors of detrital material could have turned to be the western zone of the Indo–Burman ranges and the Ganges–Brahmaputra. Such a change could be attributed to a shift of the sea surface circulation pattern between the LGM and the Holocene periods. The present-day sea surface currents have seasonal reversals in direction and intensity driven by the change in the wind pattern associated to the Indian monsoon reversal. In the Bay of Bengal, during the winter (summer) months, the surface circulation is strongly cyclonic (anticyclonic). Hydrological reconstructions of the major sea surface current suggest that during the LGM the summer monsoon was weaker than today and, on the contrary, the NE monsoon was stronger [11–13]. Such an increase of the NE monsoon then drives a similar change of the mean annual sea surface circulation pattern. So during the LGM, a tongue-shaped body of low-salinity water rich in terrestrial organic carbon appears in the eastern Bay of Bengal and the Andaman Sea [11,12], spatially correlated with the tongue-shaped Sr–Nd isotopic domain defined above. Concomitant changes of the dominant sea surface circulation may have the following consequences: during the Holocene, the dominant mean annual water circulation is anticyclonic, which, in the 'tongue', lowers the Arakan coast contribution relative to the Himalayan and Irrawaddy contribution; during the LGM, the dominant mean annual water circulation turns to cyclonic, which still insures a minute contribution of Himalayan material, but switches the Irrawaddy off and the Arakan coast on (Figs. 4 and 9). Such impact of the dominant sea surface circulation changes on the sedimentary transport would imply that the deposit velocity in the water column is very low to insure that the riverine particulates stay in the surface water column long enough.

However, a climate-related change of the $^{87}Sr/^{86}Sr$ ratio of the detrital material carried by the Himalayan rivers to the Bay of Bengal cannot be excluded from the available data. Glacial sediments are known to have more primary Sr isotopic characteristics [28,29] and by consequence could have higher $^{87}Sr/^{86}Sr$ ratios in the Himalayan area. To confirm such impact, it is necessary to establish changes of the weathering intensity during glacial/interglacial cycles.

5.3. Clay mineralogy and climatic changes

Analysis of the clay size fraction by transmission electron microscopy coupled with spectroscopy

analysis (JEOL 200C) shows that in both cores the nature and chemical composition of the clay minerals do not change with burial. This indicates that the clay minerals are not affected by early diagenesis, which is consistent with previous studies from the Bay of Bengal and Andaman Sea sediments [25,30]. Thus changes in the composition of clay mineral associations reflect those of the terrigenous supply.

Origins and source areas of the Bengal Fan clay minerals have been documented by mineralogical [3,25,30] and isotopic [3,6,8,10] studies. Both illite and chlorite may derive either from the degradation of muscovite and biotite of metamorphic and igneous formations or from the erosion of sedimentary rocks. Chlorite is also a common 'primary' mineral of low-grade metamorphic rocks. Consequently, illite and chlorite can be considered as mainly primary minerals, deriving from physical erosion or moderate chemical weathering and glacial scour such as those that are common in crystalline areas of the high Himalaya. Both smectite and kaolinite are formed by the hydrolysis of Himalayan minerals in the Indo–Gangetic flood plain soils where Himalayan material is deposited and altered [3,6,10].

Given the similarities in lithology and climate, it can be reasonably assumed that the Irrawaddy River basin behaves in the same way as the Indo–Gangetic area. Detrital illite, chlorite and quartz are probably produced from physical erosion of igneous, metamorphic and sedimentary formations of the highland Irrawaddy basin, while the source of kaolinite and smectite is located in the downstream parts of the catchment where ferralitic soils with more than 50% kaolinite are known [31]. An additional source of smectites may be found in the weathering products of the granodioritic–basaltic suites of the late Mesozoic–Cenozoic volcanic arc extending from the Inner Volcanic Arc of Burma down to the Andaman Sea into the Inner-Burman Tertiary basin [27]. Given the low volume of such volcanic rocks, this potential source is unlikely to be a significant contributor to the Andaman Sea sedimentation.

Consequently, smectite/(illite + chlorite) and kaolinite/quartz ratios can be used as proxies of the intensity of chemical weathering of SW Asia. A compilation of clay mineralogy records [25,30,32] is presented in Fig. 10. In the Bay of Bengal, cores MD77-180 and MD77-183 have similar clay mineralogy patterns with interglacial isotopic stages 1 and 5 characterized by higher smectite/(illite + chlorite) ratio than glacial stages 2, 3, 4 and 6 [32]. The core MD77-186, recovered from shallow water (890 m) near the Andaman and Nicobar islands, shows a higher smectite content than the other cores (Fig. 10) [30]. In core RC12-344, the Holocene is characterized by higher smectite/(illite + chlorite) ratio than glacial stages 2 and 3 (Fig. 10) [30]. Such variations suggest an increased physical weathering in SW Asia during the glacial stages (2, 3, 4 and 6). This is in agreement with the higher sedimentation rates observed during the glacial stages of core MD77-180 (Fig. 3).

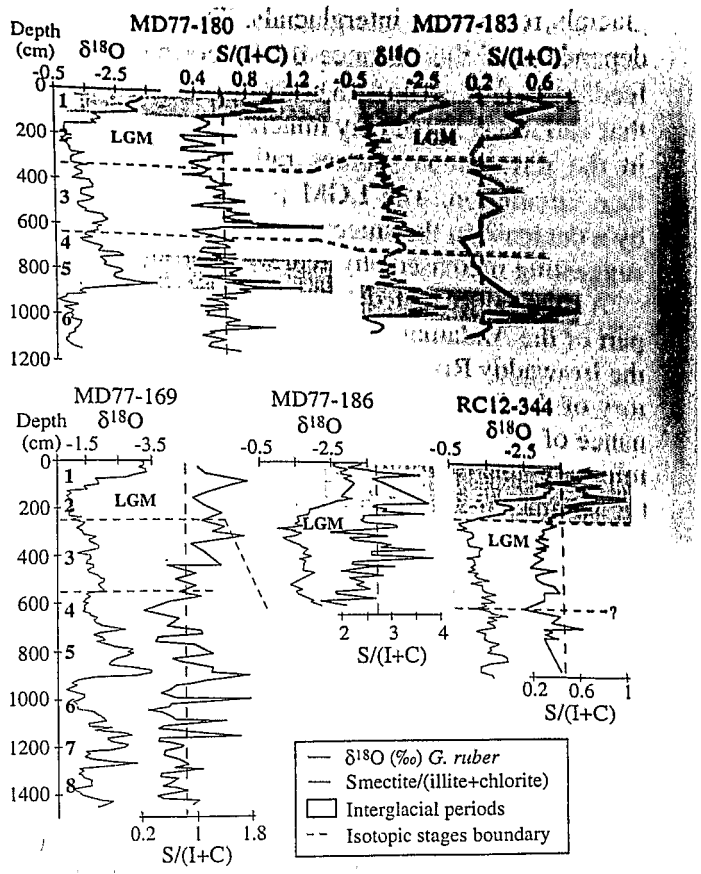

Fig. 10. $\delta^{18}O$ of *G. ruber* and smectite/(illite + chlorite) ratio versus depth (cm) for cores: MD77-169 and MD77-180 (present work); RC12-344 and MD77-186 [25,30]; MD77-183 [32]. Isotopic stages are also reported.

The conclusion is that although detrital sediments from the Bay of Bengal and Andaman Sea present different clay distributions, they generally show lower smectite/(illite + chlorite) ratios during

glacials relative to interglacials. This feature is independent of the distance of the coring site to the feeding river mouth. As a consequence, we conclude that variations in the clay mineralogy reflect changes in the terrigenous sources rather than in sea surface circulation. The LGM period is characterized by a decrease in the smectite/(illite + chlorite) ratio, suggesting increased physical weathering.

As the source of detrital material to the central part of the Andaman Sea (core MD77-169) is clearly the Irrawaddy River (Figs. 4 and 9), the erosional history of the Burman can be reconstructed. The dominance of the precessional periodicity observed in the mineralogical distribution indicates that variations in the summer monsoon intensity, rather than sea level changes, are the main control of the clay mineral assemblage fluctuations observed in the Andaman Sea sediments. In addition, glacial/interglacial changes are not characterized by changes in sedimentation rates at MD77-169 (Fig. 3).

We have reported on the the salinity gradient between the Andaman Sea and Banda Sea (see curve in Fig. 6d) as obtained by Ahmad et al. [33]. This curve has been established on the $\delta^{18}O$ difference of *G. Ruber*, a planktonic foraminifer, between cores MD77-169 and SHI90-14 (Banda Sea, water depth of 3163 m, 5°46′S 126°58′E). It gives the relative variations of the salinity of Andaman Sea surface water compared to the Banda Sea. A peak on this curve suggests a reduction of the salinity of Andaman Sea surface water related to an increase in the summer monsoon precipitation rate on the Indo–Burman river system and in the Andaman Sea. In core MD77-169, summer monsoon reinforcement is characterized by an increase of the smectite/(illite + chlorite) and kaolinite/quartz ratios. During wet periods of summer monsoon reinforcement, the vegetational cover increases in flood plain areas. This favors soil development and thus the production of smectite and kaolinite minerals, supplied to the river by low-altitude tributaries. During drier periods, the vegetational cover decreases as well as the production of pedogenic clays in the plain and the detrital material issued from the physical erosion of the high Himalaya, having experienced a lower chemical weathering, becomes predominant. This view is confirmed by the major element geochemistry which indicates that peaks of smectite/(illite + chlorite) and kaolinite/quartz are correlated to high values of the CIA* reflecting a more intense weathering (Fig. 6b).

6. Summary and conclusions

Both Nd and Sr isotope composition and clay mineralogy constrain sediment sources to the Bay of Bengal and Andaman Sea and permit a reconstruction of the erosional history of the Indo–Burman ranges.

(1) The Nd and Sr geographical distribution shows several sources for the Bay of Bengal and Andaman Sea sediments. The western Bay of Bengal is mainly supplied by the Ganges/Brahmaputra rivers, whereas sediment from the eastern Bay of Bengal results from the mixing of material from the Himalayan and Indo–Burman ranges. The Andaman Sea is mainly fed by the Irrawaddy River detrital input.

(2) The LGM sediments of the Andaman Sea and the Bay of Bengal are characterized by a significant increase in $^{87}Sr/^{86}Sr$ with a little change in $\varepsilon_{Nd}(0)$. This Sr isotopic composition change is associated with a decrease of the smectite/(illite + chlorite) ratio suggesting a decrease of chemical weathering. These variations can be attributed to a $^{87}Sr/^{86}Sr$ change of the detrital material carried by the Indo–Burman rivers to the Bay of Bengal and the Andaman Sea. Radiogenic $^{87}Sr^{2+}$ ions created from $^{87}Rb^{+}$ are located in a different lattice configuration than the non-radiogenic Sr ions incorporated during the primary crystallization of the mineral, the so-called 'initial Sr'. As a consequence, Rb-rich minerals will have a tendency to release preferentially ^{87}Sr during weathering.

(3) Sediments from the central part of the Andaman Sea (MD77-169) appear to be ideally situated to study the erosion of the Burman ranges. Mineralogical proxies and chemical index alteration variations are characterized by a strong 23 kyr periodicity. The smectite/(illite + chlorite) and kaolinite/quartz ratios are forced by the summer monsoon changes. During wet periods of summer monsoon reinforcement, the chemical weathering of the Irrawaddy plain soils relative to physical erosion of the high Burman ranges increase. The production of pedogenic clays

in the plain (smectite and kaolinite) increases relative to detrital minerals (chlorite, kaolinite and quartz).

Acknowledgements

We wish to thank Carlo Laj and Dominique Blamart for helpful discussions and comments. The two anonymous reviewers are also thanked for constructive comments on the manuscript. We are also grateful to Eric Robin who helped during the analyses of major elements. This is LSCE contribution No. 0290. *[RV]*

References

[1] J.D. Milliman, R.H. Meade, World-wide delivery of river sediment to the oceans, J. Geol. 91 (1983) 1–21.
[2] M.M. Sarin, S. Krishnaswami, K. Dilli, B.L.K. Somayajulu, W.S. Moore, Major ion chemistry of the Ganga–Brahmaputra river system: weathering processes and fluxes to the Bay of Bengal, Geochim. Cosmochim. Acta 53 (1989) 997–1009.
[3] A. Bouquillon, C. France-Lanord, A. Michard, J.J. Tiercelin, Sedimentology and isotopic chemistry of the Bengal Fan sediments: the denudation of the Himalaya, Proc. ODP Sci. Results 116 (1990) 43–58.
[4] G.W. Brass, C.V. Raman, Clay mineralogy of sediments from the Bengal Fan, Proc. ODP Sci. Results 116 (1990) 35–41.
[5] D.W. Burbank, L.A. Derry, C. France-Lanord, Reduced Himalayan sediment production 8 Myr ago despite an intensified monsoon, Nature 364 (1993) 48–50.
[6] C. France-Lanord, L. Derry, A. Michard, Evolution of the Himalaya since Miocene time: isotopic and sedimentologic evidence from the Bengal Fan, in: P.J. Treloar, M. Searle (Eds.), Himalayan Tectonics, Geol. Soc. London Spec. Publ. 74 (1993) 603–621.
[7] N. Fagel, P. Debrabant, L. André, Clay supplies in the Central Indian Basin since the late Miocene: climatic or tectonic control?, Mar. Geol. 122 (1994) 151–172.
[8] C. France-Lanord, L.A. Derry, $\delta^{13}C$ of organic carbon in the Bengal Fan: Source evolution and transport of C_3 and C_4 plant carbon to marine sediments, Geochim. Cosmochim. Acta 58 (1994) 4809–4814.
[9] L.A. Derry, C. France-Lanord, Neogene growth of the sedimentary organic carbon reservoir, Paleoceanograpy (1999) (in press).
[10] L.A. Derry, C. France-Lanord, Neogene Himalayan weathering history and river $^{87}Sr/^{86}Sr$: impact on the marine Sr record, Earth Planet. Sci. Lett. 142 (1996) 59–74.
[11] J.-C. Duplessy, Glacial to interglacial contrasts in the northern Indian Ocean, Nature 295 (1982) 494–498.
[12] M. Fontugne, J.-C. Duplessy, Variations of the monsoon regime during the upper Quaternary: evidence from carbon isotopic record of organic matter in North Indian Ocean sediment cores, Palaeogeogr., Palaeoclimatol., Palaeoecol. 56 (1986) 69–88.
[13] A. Sarkar, R. Ramesh, S.K. Bhattacharya, G. Rajagopalan, Oxygen isotope evidence for a stronger winter monsoon current during the last glaciation, Nature 343 (1990) 549–551.
[14] S.C. Clemens, W. Prell, D. Murray, G. Shimmield, G. Weedon, Forcing mechanisms of the Indian Ocean monsoon, Nature 353 (1991) 720–725.
[15] T. Holtzapffel, Les minéraux argileux, préparation, analyse diffractométriques et détermination, Soc. Géol. Nord, Publ. 12 (1985).
[16] C. Pichard, F. Fröhlich, Analyses IR quantitatives des sédiments: exemple du dosage du quartz et de la calcite, Rev. Inst. Fr. Pét. 41 (1986) 809–819.
[17] C. Colin, C. Kissel, D. Blamart, L. Turpin, Magnetic properties of sediments in the Bay of Bengal and the Andaman Sea: impact of rapid North Atlantic Ocean climatic events on the strength of the Indian monsoon, Earth Planet. Sci. Lett. 160 (1998) 632–635.
[18] D. Ninkovich, N.J. Shackleton, A.A. Abdel-Monem, J.D. Obradovich, G. Izett, K–Ar age of the Late Pleistocene eruption of Toba, North Sumatra, Nature 276 (1978) 574–577.
[19] W.I. Rose, C.A. Chesner, Dispersal of ash in the great Toba eruption, 75 Ka, Geology 15 (1987) 913–917.
[20] S.J. Goldstein, S.B. Jacobsen, Nd and Sr isotopic systematic of river water suspended material: implications for crustal evolution, Earth Planet. Sci. Lett. 87 (1988) 215–221.
[21] D. Paillard, L. Labeyrie, P. Yiou, Analyseries 1.0: a Macintosh software for the analysis of geographical time-series, Eos 77 (1996) 379.
[22] H.W. Nesbitt, G.M. Young, Early Proterozoic climates and plate motions inferred from major element chemistry of lutites, Nature 299 (1982) 715–717.
[23] A. Galy, C. France-Lanord, L.A. Derry, The Late Oligocene–Early Miocene Himalayan belt constraints deduced from isotopic compositions of Early Miocene turbidites in the Bengal Fan, Tectonophysics 260 (1996) 109–118.
[24] V. Subramanian, Mineralogical input of suspended matter by Indian rivers into the adjacent areas of the Indian Ocean, Mar. Geol. 36 (1980) M29–M34.
[25] A. Bouquillon, H. Chamley, F. Fröhlich, Sédimentation argileuse au Cénozoique supérieur dans l'Océan Indien nord-oriental, Oceanol. Acta 12 (1989) 133–147.
[26] N.P. Wijayananda, D.S. Cronan, The geochemistry and mineralogy of marine sediments from the eastern Indian Ocean, Mar. Geol. (1994) 275–285.
[27] F. Bender, Geology of Burma, Borntraeger, Berlin, 1983.
[28] J.D. Blum, Y. Erel, K. Brown, $^{87}Sr/^{86}Sr$ ratios of Sierra Nevada stream waters: implications for relative mineral weathering rates, Geochim. Cosmochim. Acta 58 (1994) 5019–5025.

[29] A.F. White, A.E. Blum, Effects of climate on chemical weathering in watersheds, Geochim. Cosmochim. Acta 59 (1995) 1729–1747.
[30] A. Bouquillon, Influences continentales et marines dans les sédiments Cénozoïques de l'Océan Indien Nord oriental, Thèse de 3ème cycle, Université des Sciences et Techniques de Lille Flandres-Artois, 1987.
[31] P. Ségalen, Les sols ferrallitiques et leur répartition géographique, 1995.
[32] N. Fang, Le contrôle climatique de la sédimentation Quaternaire récente dans la région moyenne du cône profond du Gange (Océan Indien), Thèse de 3ème cycle, Paris VI, 1987.
[33] S.M. Ahmad, F. Guichard, K. Hardjawidjaksana, M.K. Adisaputra, L.D. Labeyrie, Late Quaternary paleoceanography of the Banda Sea, Mar. Geol. 122 (1995) 385–397.
[34] D.G. Martinson, N.G. Pisias, J.D. Hays, J. Imbrie, T.C. Moore, N.J. Shackleton, Age dating and the orbital theory of the ice ages: development of a hight resolution 0 to 300,000 yr chronostratigraphy, Quat. Res. 27 (1987) 1–29.
[35] S.B. Jacobsen, G.J. Wasserburg, Sm–Nd isotopic evolution of chondrites, Earth Planet. Sci. Lett. 50 (1980) 139.